

Sat2Flow: A Structure-Aware Diffusion Framework for Human Flow Generation from Satellite Imagery

Xiangxu Wang¹, Tianhong Zhao¹, Wei Tu², Bowen Zhang¹, Guanzhou Chen³, Jinzhou Cao^{1*}

¹College of Big Data and Internet, Shenzhen Technology University, China

²Department of Urban Informatics, School of Architecture and Urban Planning, Shenzhen University, China

³State Key Laboratory of Information Engineering in Surveying, Mapping, and Remote Sensing, Wuhan University, China
2310413035@stumail.sztu.edu.cn, zhaotianhong@sztu.edu.cn, tuwei@szu.edu.cn,
zhang_bo_wen@foxmail.com, cgz@whu.edu.cn, caojinzhou@sztu.edu.cn

Abstract

Origin-Destination (OD) flow matrices are essential for urban mobility analysis, underpinning applications in traffic forecasting, infrastructure planning, and policy design. However, existing methods suffer from two critical limitations: (1) reliance on auxiliary features (e.g., Points of Interest, socioeconomic statistics) that are costly to collect and have limited spatial coverage; and (2) sensitivity to spatial topology, where minor index reordering of urban regions (e.g., census tract relabeling) disrupts structural coherence in generated flows. To address these challenges, we propose Sat2Flow, a latent structure-aware diffusion-based framework that generates structurally coherent OD flows using solely satellite imagery as input. Our approach introduces a multi-kernel encoder to capture diverse regional interactions and employs a permutation-aware diffusion process that aligns latent representations across different regional orderings. Through a joint contrastive training objective that bridges satellite-derived features with OD patterns, combined with equivariant diffusion training that enforces structural consistency, Sat2Flow ensures topological robustness under arbitrary regional reindexing. Experimental results on real-world urban datasets demonstrate that Sat2Flow outperforms both physics-based and data-driven baselines in numerical accuracy while preserving empirical distributions and spatial structures under index permutations. Sat2Flow offers a globally scalable solution for OD flow generation in data-scarce urban environments, eliminating region-specific auxiliary data dependencies while maintaining structural invariance for robust mobility modeling.

Code — <https://github.com/5hawnWang/Sat2Flow>

Introduction

Accurate generation of origin-destination (OD) flows is fundamental to urban mobility planning (Joubert and De Waal 2020), congestion management (Iqbal et al. 2014), and public resource allocation (Rong et al. 2023). Traditional OD modeling relies heavily on infrastructure sensors (e.g., traffic counters) and travel surveys, which suffer from sparse spatial coverage and high deployment costs (Calabrese et al.

2011). Early physical models, such as gravity models (Barbosa et al. 2018) operating at the pair-wise level, provided theoretical frameworks but oversimplified urban complexity. With the advancement of machine learning, data-driven approaches have significantly improved prediction accuracy by leveraging matrix-wise level features as inputs, yet they face critical bottlenecks in data accessibility and structural modeling constraints (Rong et al. 2023; Yan et al. 2024). Current state-of-the-art frameworks exhibit two fundamental limitations:

Feature Dependency Dilemma. Existing models universally require socio-economic indicators (e.g., population density) and points-of-interest (POI) distributions as essential inputs (Cao et al. 2025a,c). These auxiliary data sources are notoriously difficult to acquire at scale due to privacy restrictions, collection costs, and inconsistent availability across different geographic regions, particularly in developing countries where urban mobility modeling is most urgently needed. In contrast, satellite imagery provides globally accessible remote sensing data that captures essential urban spatial patterns (Mohanty et al. 2020) without requiring region-specific collection or privacy-sensitive information, offering a scalable alternative to feature-dependent approaches.

Structural Consistency Deficiency. As illustrated in Figure 1, urban OD flow matrices should exhibit structural consistency under different data transformations. When the same urban area undergoes geometric transformations such as rotation, translation, or scaling (Figure 1a), the spatial relationships remain isomorphic to the original configuration. In computational representation, this geometric invariance corresponds to index permutation—reassigning the regional index while maintaining identical connectivity patterns (Figure 1b). However, conventional models fail to recognize this equivalence, treating permuted representations as distinct inputs despite encoding identical mobility relationships. This fundamental limitation reveals the absence of structural consistency (i.e., permutation equivariance in computational representation) in existing approaches.

To address these fundamental limitations, we propose **Sat2Flow** – a permutation-equivariant framework for generating urban OD flows using globally accessible satellite imagery as the sole input modality. This approach eliminates

*Corresponding author.

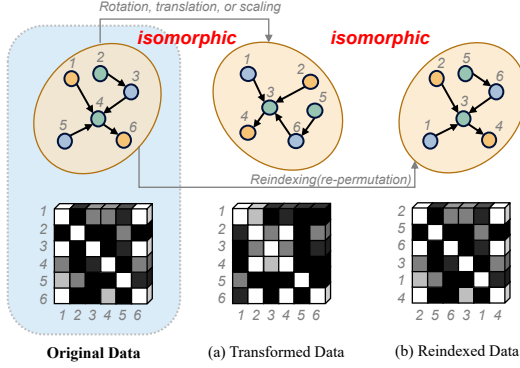


Figure 1: Structural consistency in urban OD flows. Geometric transformations (a) and index permutations (b) preserve isomorphic spatial relationships, maintaining structural consistency under regional reindexing.

dependency on scarce auxiliary data by extracting multi-scale urban patterns directly from remote sensing imagery, while ensuring structural consistency and enabling reliable deployment across diverse urban environments worldwide. The framework operates through three sequential stages: The first stage establishes a systematic pipeline for downloading satellite imagery of urban regions and encoding them into feature representations. The second stage processes the encoded region features through multi-kernel computing to generate a multi-kernel (MK) matrix, then employs two architecturally identical encoders to align the MK matrix and OD matrix in a shared latent space through pre-training the proposed **Modality-Joint Contrastive Module**. The third stage utilizes the aligned regional multi-kernel representation from the latent space, along with permutation embedding, as conditional inputs to a novel **Conditional Latent Diffusion Module**. This module progressively denoises latent variables to synthesize structurally consistent origin-destination flow matrices. Our contributions are:

- We present the first OD flow generation solution using only satellite imagery, eliminating dependencies on scarce region-specific auxiliary data while maintaining competitive performance.
- We develop an adaptive encoder based on multi-kernel functions for regional representation from satellite imagery, capturing local urban features and global spatial dependencies without manual feature engineering.
- We introduce a conditional latent diffusion module with permutation embeddings that ensures structural consistency under arbitrary regional index reordering, addressing a key limitation in existing approaches.
- Experiments on 3,333 U.S urban areas demonstrate the state-of-the-art performance of Sat2Flow, showing superior scalability and global applicability.

Primaries

Definition 1. (Urban Region). A city is partitioned into N distinct urban regions $\mathcal{R} = \{r_i\}_{i=1}^N$, where each region r_i

corresponds to a geographically defined unit such as a census tract or administrative division.

Definition 2. (Satellite Imagery). Satellite imagery \mathcal{I} comprises high-resolution remote sensing data that capture geospatial features across urban landscapes. For each region r_i , we extract a georeferenced image $\mathbf{I}_i \in \mathbb{R}^{h \times w \times c}$ with spatial dimensions h and w , which preserves multispectral attributes and ground-level structural patterns.

Definition 2. (OD Flow). Origin-Destination (OD) flow is formalized as a set of ordered triples $\{(r_o, r_d, M_{r_o \rightarrow r_d})\}$, where r_o and r_d denote origin and destination regions, and $M_{r_o \rightarrow r_d}$ quantifies the intensity of mobility between these regions. This flow can also be represented as a matrix $\mathbf{M} \in \mathbb{R}^{N \times N}$, or interpreted as a single-channel image with $N \times N$ spatial resolution.

Definition 3. (Kernel Function). A kernel function $\kappa(\cdot, \cdot)$ is defined on a Reproducing Kernel Hilbert Space (RKHS) \mathcal{H} , where it serves as a similarity measure between feature vectors $\mathbf{x}_i, \mathbf{x}_j \in \mathcal{X}$. The kernel satisfies:

$$\kappa(\mathbf{x}_i, \mathbf{x}_j) = \langle \phi(\mathbf{x}_i), \phi(\mathbf{x}_j) \rangle_{\mathcal{H}} = \phi(\mathbf{x}_i)^\top \phi(\mathbf{x}_j),$$

where $\phi(\cdot) : \mathcal{X} \mapsto \mathcal{H}$ is an implicit feature mapping that embeds the input feature space into RKHS. This formulation ensures that $\kappa(\cdot, \cdot)$ is symmetric and positive semi-definite, aligning with Mercer’s theorem and enabling kernel methods for spatial analysis.

Definition 4. (Permutation Equivariant). A generative model \mathcal{G} is permutation-equivariant if, for any permutation π of urban regions, the generated OD matrix $\mathbf{M}' = \mathcal{G}(\{\mathbf{x}_{\pi(i)}\}_{i=1}^N)$ satisfies:

$$[\mathbf{M}']_{i,j} = [\mathbf{M}]_{\pi(i), \pi(j)},$$

where $\mathbf{M} = \mathcal{G}(\{\mathbf{x}_i\}_{i=1}^N)$ is the original output matrix. This property ensures that the model’s predictions are structurally consistent with input permutations, preserving topological relationships under reordering.

Problem Formulation (OD Flow Generation). Given a set of regional feature vectors $\{\mathbf{x}_i | r_i \in \mathcal{R}\}_{i=1}^N \in \mathbb{R}^{N \times d}$, the goal is to learn a permutation-equivariant conditional generative model \mathcal{G} that reconstructs the OD flow matrix $\mathbf{M} \in \mathbb{R}^{N \times N}$.

Methodology

This section elaborates on Sat2Flow, which is a three-stage framework for OD flow generation, as illustrated in Figure 2. First, satellite image tiles are collected for urban regions and encoded into feature vectors via a pre-trained vision encoder, forming an embedding database. Next, a modality-Joint contrastive module aligns regional multi-kernel representations and OD flow representations in a shared latent space through dedicated encoders and contrastive learning. Finally, a conditional latent diffusion module is trained to generate OD matrices conditioned on the latent presentations and permutation embeddings, ensuring structural consistency under input reordering.

Satellite Imagery Encoding

Sat2Flow constructs a satellite imagery database by systematically collecting and pre-processing georeferenced image

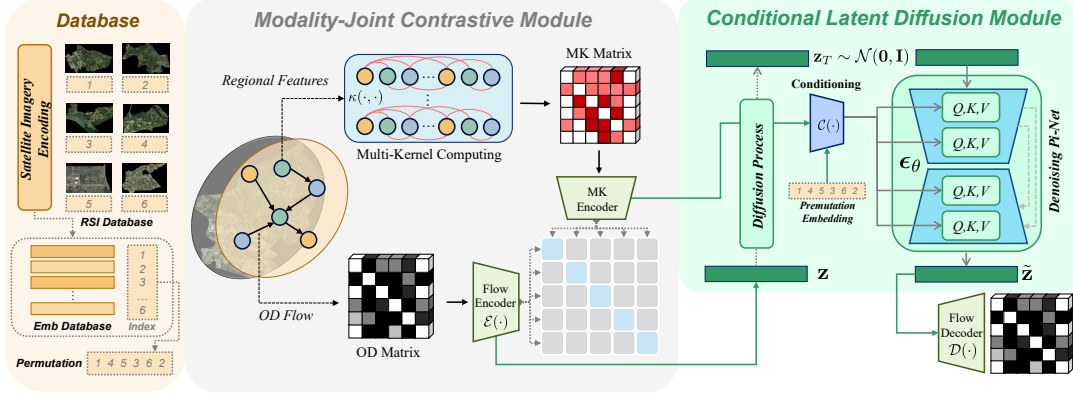


Figure 2: Overview of the Sat2Flow framework, featuring three sequential stages (satellite encoding, multi-kernel contrastive learning, and diffusion generation), with the latter two stages integrated within the Modality-Joint Contrastive Module and Conditional Latent Diffusion Module, respectively.

tiles for each urban region $r_i \in \mathcal{R}$. The process begins with identifying and downloading high-resolution tiles from standardized imagery services (e.g., Esri World Imagery or Google Earth Engine) that correspond to the geographical boundaries of region r_i . To ensure spatial fidelity, these tiles are cropped and aligned with the exact contours of each region while preserving their original regional indices. The indexing scheme establishes a bijective mapping between each image $\mathbf{I}_i \in \mathbb{R}^{h \times w \times c}$ and its associated region r_i , ensuring structural consistency during arbitrary re-indexing operations.

The preprocessed satellite imagery is subsequently encoded into semantic feature representations using a pre-trained vision encoder. Given the complexity and high dimensionality of raw pixel data, which often contains redundant textures and environmental noise, we adopt RemoteCLIP (Liu et al. 2024), a vision-language model specifically designed for satellite imagery analysis. The encoder transforms each image patch \mathbf{I}_i to a high-dimensional feature vector \mathbf{x}_i . The resulting embeddings $\{\mathbf{x}_i\}_{i=1}^N$ are stored in a structured embedding database with indices preserved from the original satellite image database. These embeddings serve as conditional input for the subsequent multi-kernel encoder and latent diffusion components, where both the regional characteristic vectors \mathbf{x}_i and permutation embeddings are jointly leveraged to generate structurally consistent and topologically robust OD flow matrices.

Modality-Joint Contrastive Module

The second stage of Sat2Flow focuses on cross-modal representation learning through a contrastive pretraining module that jointly encodes OD flows and regional feature vectors. By aligning the latent representations of OD patterns and urban semantics in a shared embedding space, serving as the foundation for the subsequent diffusion-based generative modeling.

Multi-Kernel Encoder The complex interactions among urban regions collectively form a city-wide relational network. To capture these latent associations, we propose

a **multi-kernel computing** method that learns region-to-region dependencies through adaptive RKHS mappings (Shawe-Taylor and Cristianini 2004), distinct from graph neural networks that rely on pre-defined adjacency matrices. Specifically, given a set of L mappings $\{\phi_l\}_{l=1}^L$, L kernel functions compute the similarity between two regions $r_i, r_j \in \mathcal{R}$:

$$[\mathbf{K}]_{i,j}^l = \kappa^l(\mathbf{x}_i, \mathbf{x}_j) = \phi_l(\mathbf{x}_i)^\top \phi_l(\mathbf{x}_j), \quad l = 1, 2, \dots, L \quad (1)$$

where $\mathbf{x}_i, \mathbf{x}_j \in \mathcal{X} \subseteq \mathbb{R}^d$ are regional feature vectors of r_i and r_j , and $\mathbf{K}^l \in \mathbb{R}^{N \times N}$ is represents the l -th relational matrix. This yields L kernel matrices $\mathbf{K}^1, \mathbf{K}^2, \dots, \mathbf{K}^L$, which encode multi-perspective interactions.

To incorporate structural priors (e.g., road network topology), an additional kernel matrix \mathbf{K}^{L+1} is constructed by leveraging domain knowledge, leading to a tensor $\mathcal{K} \in \mathbb{R}^{N \times N \times (L+1)}$ through concatenation:

$$\mathcal{K} = \text{Concat}(\mathbf{K}^1, \mathbf{K}^2, \dots, \mathbf{K}^L, \mathbf{K}^{L+1}). \quad (2)$$

This tensor is treated as a multi-channel image with spatial dimensions $N \times N$, where each channel corresponds to a distinct relational prior. Subsequently, an attention-augmented encoder (MK Encoder) is used to process the multichannel relational tensor \mathcal{K} , producing a regional multi-kernel representation \mathbf{z}_c . This representation serves a dual role: It is first aligned with the OD representation in a shared latent space through contrastive learning, enforcing semantic consistency between regional interaction patterns and mobility dynamics; subsequently, \mathbf{z}_c is integrated as a conditional input to the diffusion module, guiding the generative process by encoding high-level spatial priors.

Flow Encoder The OD flow matrix is interpreted as a single-channel spatial map with resolution $N \times N$, where N varies between cities due to different regional divisions. This spatial regularity enables convolutional neural networks to effectively capture hierarchical dependencies. The translation-equivariant property of convolutions further ensures robustness to permutations of region indexing. We em-

ploy an attention-augmented convolutional Variational Autoencoder with a fully convolutional architecture, enabling processing of variable-sized inputs (e.g., cities with differing N) through dynamic padding or interpolation. An encoder-decoder pair will be trained synchronously, where the encoder $\mathcal{E}(\cdot)$, termed the Flow Encoder, shares the same architecture as the MK Encoder to model the approximate posterior distribution $q_z(\mathbf{z}|\mathbf{M})$ of the latent variable \mathbf{z} , while the Flow Decoder $\mathcal{D}(\cdot)$ adopts a symmetric design effectively reconstructing the OD matrix through the generative distribution $p_\theta(\mathbf{M}|\mathbf{z})$. The encoder and decoder architecture closely resembles the subsequent Pi-net structure detailed in Figure 3.

Latent Aligned Training To bridge the modality gap between regional features and OD flows, we adopt a CLIP-style modality alignment objective that enforces mutual alignment between latent representations \mathbf{z}_c (from the MK Encoder) and \mathbf{z} (from the Flow Encoder) in the shared latent space. This contrastive loss \mathcal{L}_{con} encourages positive pairs (matching MK-OD samples) to cluster closely while pushing negative pairs apart, formalized as:

$$\mathcal{L}_{\text{con}} = -\frac{1}{2N_B} \left(\sum_{i=1}^{N_B} \log \frac{\exp(\text{sim}(\mathbf{z}^{(i)}, \mathbf{z}_c^{(i)})/\tau)}{\sum_{j=1}^N \exp(\text{sim}(\mathbf{z}^{(i)}, \mathbf{z}_c^{(j)})/\tau)} + \sum_{i=1}^{N_B} \log \frac{\exp(\text{sim}(\mathbf{z}_c^{(i)}, \mathbf{z}^{(i)})/\tau)}{\sum_{j=1}^{N_B} \exp(\text{sim}(\mathbf{z}_c^{(i)}, \mathbf{z}^{(j)})/\tau)} \right), \quad (4)$$

where $\text{sim}(\cdot, \cdot)$ denotes the cosine similarity, τ is the temperature parameter, and N_B represents the number of MK-OD pairs in a mini-batch.

In parallel, a reconstruction loss is introduced to ensure fidelity in the generative process:

$$\mathcal{L}_{\text{rec}} = -\mathbb{E}_{\mathbf{z} \sim q_z(\mathbf{z}|\mathbf{M})} \log p_\theta(\mathbf{M}|\mathbf{z}), \quad (4)$$

which reduces to a pixel-wise ℓ_2 loss when the decoder follows an isotropic Gaussian distribution.

To further regularize the latent space, we incorporate a Kullback-Leibler (KL) divergence term that aligns the encoder output distribution $q_z(\mathbf{z}|\mathbf{M})$ with a standard Gaussian prior:

$$\mathcal{L}_{\text{KL}} = D_{\text{KL}}(q_z(\mathbf{z}|\mathbf{M}) \parallel \mathcal{N}(0, \mathbf{I})). \quad (5)$$

This encourages the latent representations to remain compact and well-distributed, preventing degenerate solutions during diffusion modeling.

The final training objective combines the contrastive loss \mathcal{L}_{con} , a reconstruction loss \mathcal{L}_{rec} and the KL loss \mathcal{L}_{KL} :

$$\mathcal{L} = \mathcal{L}_{\text{rec}} + \alpha \mathcal{L}_{\text{con}} + \beta \mathcal{L}_{\text{KL}} \quad (6)$$

where α and β are hyperparameters that balance the contributions of the contrastive and KL regularization terms relative to the reconstruction loss.

Conditional Latent Diffusion Module

Building upon the latent representation learned in the contrastive module, this stage introduces a latent diffusion model (Rombach et al. 2022) that generates OD flow matrices conditioned on urban regional multi-kernel representation and permutation embeddings.

Permutation Embedding To ensure structural coherence in OD generation under arbitrary region permutations, we introduce permutation embeddings that encode explicit structural priors into the denoising process. Formally, we maintain a learnable lookup table $\mathbf{E} \in \mathbb{R}^{N \times d}$, where each row \mathbf{e}_i corresponds to the embedding of the original index i . For a given permutation π , the reordered index sequence $\pi(1), \pi(2), \dots, \pi(N)$ retrieves the corresponding embeddings:

$$\mathbf{z}_p = \text{MLP}(\text{Concat}(\mathbf{e}_{\pi(1)}, \dots, \mathbf{e}_{\pi(N)})),$$

where $\mathbf{z}_p \in \mathbb{R}^{d_c}$ serves as the permutation-aware condition for the diffusion model. This design explicitly guides the generator to respect the structural relationships among regions during OD flow generation.

Denoising Pi-Net Backbone The diffusion process follows a standard Markov chain formulation, where noise is progressively added over T steps to transform the latent OD representation into a sample from the prior distribution $\mathbf{z}_T \sim \mathcal{N}(0, \mathbf{I})$:

$$q(\mathbf{z}_t | \mathbf{z}_{t-1}) = \mathcal{N}(\mathbf{z}_t; \sqrt{1 - \beta_t} \mathbf{z}_{t-1}, \beta_t \mathbf{I}), \quad t = 1, 2, \dots, T. \quad (7)$$

The reverse process, governed by the neural backbone, aims to recover $\tilde{\mathbf{z}} = \mathbf{z}$ from \mathbf{z}_T and conditions $\mathcal{C} = \{\mathbf{z}_c, \mathbf{z}_p\}$ by learning to estimate the noise added at each step:

$$p_\theta(\mathbf{z}_{t-1} | \mathbf{z}_t, \mathcal{C}) = \mathcal{N}(\mathbf{z}_{t-1}; \boldsymbol{\mu}_\theta(\mathbf{z}_t, \mathcal{C}, t), \boldsymbol{\Sigma}_\theta(\mathbf{z}_t, \mathcal{C}, t)), \quad (8)$$

where

$$\boldsymbol{\mu}_\theta(\mathbf{z}_t, \mathcal{C}, t) = \frac{1}{\sqrt{\alpha_t}} \left(\mathbf{z}_t - \frac{1 - \alpha_t}{\sqrt{1 - \bar{\alpha}_t}} \boldsymbol{\epsilon}_\theta(\mathbf{z}_t, \mathcal{C}, t) \right), \quad (9)$$

with $\alpha_t = 1 - \beta_t$, and $\bar{\alpha}_t = \prod_{i=1}^t \alpha_i$ representing the noise schedules provided in (Ho, Jain, and Abbeel 2020; Song, Meng, and Ermon 2020).

Pi-Net. We propose Pi-Net—a variant of U-Net with an inverted encoder-decoder structure that estimates noise $\boldsymbol{\epsilon}_\theta(\mathbf{z}_t, \mathcal{C}, t)$ through parameters θ . Unlike conventional U-Net architectures that follow a downsample-then-upsample paradigm, Pi-Net adopts an up-then-down approach to address the unique characteristics of OD matrices, as illustrated in Figure 3. Specifically, the network first performs upsampling to expand spatial resolution, enabling explicit modeling of intermediate mobility patterns between regions (e.g., virtual transit hubs r_v connecting r_i to r_j), before applying downsampling to refine global coherence. This design ensures that latent codes at high resolutions retain fine-grained interaction details, which are critical for capturing spatial dependencies in OD flows.

Condition Injection. The regional multi-kernel representation \mathbf{z}_c and permutation embedding \mathbf{z}_p are injected into the

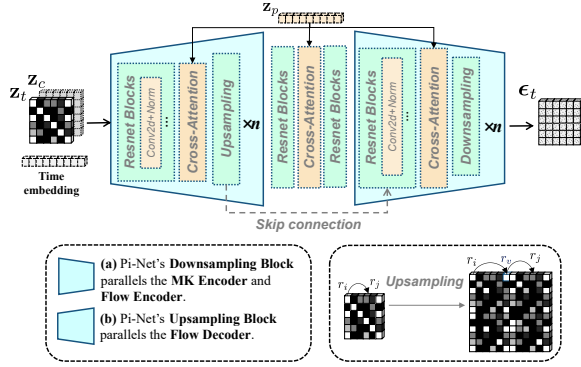


Figure 3: Pi-Net Architecture: Inverted U-Net Design for OD Flow Generation.

diffusion model through distinct mechanisms optimized for their respective characteristics. Given that z_c shares the same spatial resolution as the latent representation z_t , it is concatenated along the channel dimension to provide spatially-aligned regional context. In contrast, z_p is integrated via a hierarchical cross-attention mechanism, acting as a structural prior to modulate spatial dependencies.

Equivariant Diffusion Training Our conditional latent diffusion module is trained with two complementary objectives. The primary objective enforces structural consistency across region index permutations: for each input sample, N_p reindexed variants are generated via random permutations, and the model must reconstruct the corresponding OD matrices while properly aligning with the associated permutation embeddings. This is formalized as:

$$\mathcal{L}_{\text{pre}} = \frac{1}{N_p} \sum_{k=1}^{N_p} \|\mathbf{M}_{\pi_k} - \mathcal{D}_{\pi_k}(\mathbf{z})\|_2^2, \quad (10)$$

where $\mathcal{D}_{\pi_k}(\mathbf{z})$ denotes the model’s reconstructed output under permutation π_k . The secondary objective maintains the standard diffusion loss for high-quality generation:

$$\mathcal{L}_{\text{LDM}} = \mathbb{E}_{\mathbf{z}, \epsilon \sim \mathcal{N}(\mathbf{0}, \mathbf{I}), t} [\|\epsilon - \epsilon_\theta(\mathbf{z}_t, \mathcal{C}, t)\|_2^2]. \quad (11)$$

Following training, the Sat2Flow supports efficient sampling from the learned latent distribution and reconstructing OD flow matrices. The sampling process is accelerated using the DDIM method (Song, Meng, and Ermon 2020), which reduces the number of denoising steps while maintaining generation quality, as detailed in Algorithm 1.

Experiments

Datasets

We evaluated our approach in the *CommutingODGen* dataset (Rong et al. 2024), which comprises 3,333 urban areas across the United States, including 3,233 counties and 100 metropolitan statistical areas. Each urban area is partitioned into fine-grained administrative units: census tracts for counties and census block groups for metropolitan regions. OD flow matrices are derived from the Longitudinal Employer-Household Dynamics Origin-Destination

Algorithm 1: OD Matrix Generation through Sat2Flow

Input

Regional satellite features $\{\mathbf{x}_i\}_{i=1}^N$ of a target city
 Permutation sequence $\pi(1), \pi(2), \dots, \pi(N)$
 Length τ of subsequence in DDIM sampling

Output

OD matrix \mathbf{M} of that target city.

- 1: Compute multi-kernel condition $\mathbf{z}_c = \mathcal{E}(\mathcal{K})$ via multi-kernel encoder with $\{\mathbf{x}_i\}_{i=1}^N$
- 2: Construct permutation embedding \mathbf{z}_p based on π
- 3: Sample $\mathbf{z}_T \sim \mathcal{N}(\mathbf{0}, \mathbf{I})$ from the prior
- 4: Set step interval $\Delta t = \lfloor T/\tau \rfloor$
- 5: **for** $t = T, T - \Delta t, \dots, \Delta t$ **do**
- 6: $\mathbf{z}_{t-\Delta t} \leftarrow \frac{1}{\sqrt{\alpha_t}} \left(\mathbf{z}_t - \frac{1-\alpha_t}{\sqrt{1-\alpha_t}} \epsilon_\theta(\mathbf{z}_t, \mathcal{C}, t) \right)$
- 7: **end for**
- 8: Reconstruct OD matrix via decoder: $\hat{\mathbf{M}} \leftarrow \mathcal{D}(\mathbf{z}_0)$
- 9: **return** $\hat{\mathbf{M}}$

Employment Statistics (LODES), a comprehensive source maintained by the U.S. Census Bureau, capturing commuting patterns between these regional units.

Baselines

We evaluated the proposed Sat2Flow framework against seven representative baselines, categorized into two modeling paradigms: physics-based and data-driven models. **Physics-based models** encompass the Gravity Model (Zipf 1946) with power-law decay (GM-P) and exponential decay (GM-E), which rely solely on the population distribution as input and are grounded in the theoretical principles of human mobility. **Data-driven models** include Random Forest (RF) (Poureira et al. 2018), DeepGravity (DGM) (Simini et al. 2021), Geo-contextual Multitask Embedding Learning (GMEL) (Liu et al. 2020), NetGAN (Bojchevski et al. 2018), and DiffODGen (Rong et al. 2023), which leverage richer semantic and structural features.

Experimental Settings

Dataset Processing The dataset is partitioned into training, validation, and test sets using an 8:1:1 split, ensuring sufficient data for model learning and unbiased evaluation. A logarithmic transformation is applied to the OD flow matrices to address their heavy-tailed distribution. This step is motivated by theoretical studies that identify power-law scaling in human mobility patterns (Saber et al. 2018).

Implementation Details The proposed Sat2Flow framework is implemented in PyTorch using the AdamW optimizer with a learning rate of 10^{-3} and weight decay of 10^{-2} . Contrastive learning and diffusion learning are trained for 1000 epochs with a batch size of 12. For data augmentation, we apply random permutations to regional indices at 50% intensity to enhance robustness to index reordering. Satellite imagery is encoded into 768-dimensional features, while the multi-kernel encoder is configured with kernel dimension 64 and 8 kernels. All experiments were performed on a single NVIDIA GeForce RTX A6000 GPU with 50GB of memory.

Model	Flow Value			Empirical Distribution (JSD)		
	CPC↑	RMSE↓	NRMSE↓	inflow↓	outflow↓	ODflow↓
GM-P	0.321	174.0	2.222	0.668	0.656	0.409
GM-E	0.329	162.9	2.080	0.652	0.637	0.422
RF	0.458	100.4	1.282	0.424	0.503	0.219
DGM	0.431	92.9	1.186	0.469	0.561	0.230
GMEL	0.440	94.3	1.204	0.445	0.355	0.207
NetGAN	0.487	89.1	1.138	0.429	0.354	0.191
DiffODGen	0.532	74.6	0.953	0.324	0.270	0.149
WeDAN	<u>0.593</u>	<u>68.6</u>	<u>0.876</u>	<u>0.291</u>	<u>0.269</u>	<u>0.147</u>
Sat2Flow	0.635 (+7.06%)	65.1 (+5.14%)	0.831 (+5.14%)	0.272 (+6.52%)	0.266 (+1.10%)	0.145 (+1.36%)

Table 1: Performance comparison with baseline models on test cities.

Model	Permutation Increases (JSD ↓)				
	10%	30%	50%	80%	100%
GMEL	0.213	0.213	0.213	0.213	0.213
NetGAN	0.206	0.210	0.221	0.225	0.231
DiffODGen	0.156	0.162	0.182	0.193	0.211
WeDAN	0.158	0.167	0.179	0.193	0.207
Sat2Flow	0.149	0.154	0.160	0.164	0.171

Table 2: Performance under progressive index permutation at varying intensities on test cities.

Evaluation Metrics To comprehensively assess the quality of generated OD matrices, we employ four complementary metrics that capture different aspects of generation fidelity. **Flow-level accuracy** is measured using three error metrics that quantify deviations in flow values: Root Mean Square Error (RMSE), Normalized Root Mean Square Error (NRMSE), and Common Part of Commuting (CPC):

$$\text{RMSE} = \sqrt{\frac{1}{N^2} \|\mathbf{M} - \hat{\mathbf{M}}\|_F^2}, \quad (12)$$

$$\text{NRMSE} = \text{RMSE} / \sqrt{\frac{1}{N^2} \|\mathbf{M} - \bar{\mathbf{M}}\|_F^2}, \quad (13)$$

$$\text{CPC} = \frac{2 \sum_{i,j} \min([\mathbf{M}]_{i,j}, [\hat{\mathbf{M}}]_{i,j})}{\sum_{i,j} [\mathbf{M}]_{i,j} + \sum_{i,j} [\hat{\mathbf{M}}]_{i,j}}, \quad (14)$$

where $\|\cdot\|_F$ denotes the Frobenius norm, and $\bar{\mathbf{M}}$ represents the mean of elements in the OD matrix \mathbf{M} .

Distributional alignment is quantified using Jensen-Shannon divergence (JSD) to measure global distributional similarity between real and generated OD matrices:

$$\text{JSD} = \frac{1}{2} D_{KL}(\mathbf{P}_{\mathbf{M}} \|\mathbf{P}_{\hat{\mathbf{M}}}) + \frac{1}{2} D_{KL}(\mathbf{P}_{\hat{\mathbf{M}}} \|\mathbf{P}_{\mathbf{M}}), \quad (15)$$

where $\mathbf{P}_{\mathbf{M}}$ and $\mathbf{P}_{\hat{\mathbf{M}}}$ represent the marginal empirical distributions of the real matrix \mathbf{M} and the generated matrix $\hat{\mathbf{M}}$, respectively.

Performance Comparison

Table 1 presents a comprehensive performance comparison between Sat2Flow and seven representative baseline models across six evaluation metrics on test cities. The experimental results reveal the following key observations: (1) Sat2Flow achieves the highest CPC of 0.635 (+7.06% over WeDAN) and lowest errors with RMSE of 65.1 and NRMSE of 0.831 (+5.14% improvement). These substantial improvements demonstrate that, with our framework, satellite imagery alone captures underlying spatial mobility patterns more effectively than traditional feature-rich approaches. (2) Our method achieves the lowest JSD across all mobility distributions. The consistent improvements across local mobility characteristics and global connectivity patterns indicate that Sat2Flow effectively preserves the statistical properties of real mobility flows. (3) Physics-based models show poor performance with CPC around 0.32, confirming their oversimplified assumptions, while data-driven models show progressive improvements. Notably, Sat2Flow surpasses even advanced feature-rich baselines, highlighting the efficacy of extracting mobility patterns directly from satellite imagery without region-specific auxiliary data.

Consistency Evaluation

To validate the structural consistency of our approach, we conduct an analysis of model performance under progressive index permutation at varying intensities (10% to 100%). Table 2 presents the distributional fidelity results measured through JSD. It is evident that pair-wise level models, represented by GMEL, inherently adapt to different index orderings as they predict flows for individual regions in isolation, with consistent JSD values of 0.213 across all permutation intensities; however, their accuracy remains limited due to the neglect of spatial interaction information. In contrast, recent matrix-wise level models, which generate city-scale multi-regional flows in a single step, capture spatial structures but exhibit sensitivity to isomorphic spatial configurations (i.e., index permutations), with performance deteriorating as permutation intensity increases. Sat2Flow demonstrates minimal performance variation under index permu-

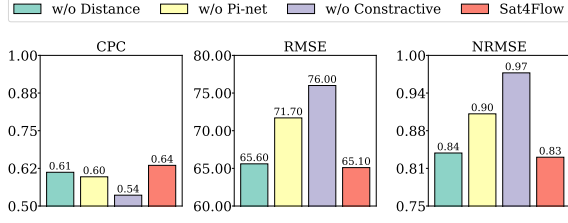


Figure 4: Ablation study evaluating component contributions through CPC, RMSE, and NRMSE metrics.

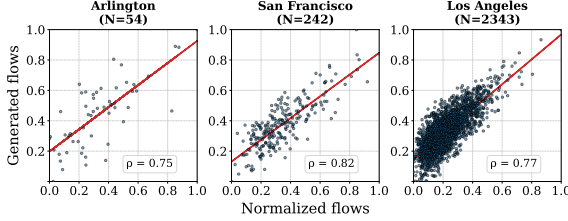


Figure 5: Case study analyzing model behavior across selected cities with diverse sizes.

tations while maintaining high accuracy, attributable to its permutation-equivariant diffusion training.

Ablation Study

To systematically evaluate the contribution of each component in Sat2Flow, we design three ablation variants by removing specific modules: **w/o Distance**: Eliminates the topological distance prior in multi-kernel encoding, removing explicit spatial relationship constraints. **w/o Pi-net**: Replaces the permutation-aware Pi-net backbone with a standard U-net architecture. **w/o Contrastive**: Removes the contrastive learning phase, disabling latent space alignment between regional representations and OD flows during the first training stage. As shown in Figure 4, the full Sat2Flow consistently outperforms all ablated variants across all metrics. **w/o Distance** achieves 65.60 RMSE, only 0.8% higher than full Sat2Flow, confirming that the multi-kernel encoder effectively captures regional relationships while demonstrating that satellite imagery inherently encodes spatial relationships without explicit distance modeling. **w/o Pi-net** shows significant degradation, demonstrating that Pi-net’s up-then-down architecture is essential for preserving intermediate mobility patterns that standard U-net misses. **w/o Contrastive** suffers the largest performance drop as eliminating the contrastive learning phase prevents the condition embeddings from being guided into a latent space aligned with OD semantic representation, forcing the model to search within a broader solution space from scratch and consequently converge to suboptimal local minima.

Case Study

We evaluate model performance across cities of varying scales by comparing generated and real OD flows, as shown in Figure 5. Three representative cities were selected: Ar-

lington, San Francisco, and Los Angeles. It can be observed that model performance peaks at medium-sized cities ($\rho = 0.82$ for San Francisco), while slightly declining for both smaller ($\rho = 0.75$ for Arlington) and larger cities ($\rho = 0.77$ for Los Angeles). This pattern aligns with the concept of urban scaling laws (Pumain et al. 2006), where medium-sized cities exhibit balanced spatial heterogeneity—not constrained by limited connectivity in small towns nor overwhelmed by excessive functional fragmentation in megacities. The consistent performance across scales confirms Sat2Flow’s robustness to urban morphology variations, while the minor dip in megacities reflects challenges in modeling long-tail mobility patterns across highly diverse areas.

Related Work

Human flow generation has progressed through distinct methodological phases, transitioning from labor-intensive data collection to automated modeling approaches (Luca et al. 2021). Early approaches relied on manual travel surveys and census data collection (Axhausen et al. 2002; Iqbal et al. 2014), which were prone to sampling bias and substantial respondent burden. Subsequent physical modeling approaches, including the gravity model (Zipf 1946) and the radiation model (Simini et al. 2012), model human mobility through population-based interactions. However, their exclusive reliance on demographic counts oversimplifies urban complexity and fails to capture nuanced socioeconomic mobility patterns inherent in modern cities (Cao et al. 2025a). The emergence of big data enabled more sophisticated modeling through comprehensive urban descriptors. Tree-based methods (Pourebrahim et al. 2019) achieved initial success, while deep learning architectures demonstrated initial success by incorporating sociodemographics, POIs, and land use patterns. Deep learning architectures further enhanced prediction accuracy by leveraging road network topology and multi-modal urban features (Wang et al. 2025). Recent advances have focused on explicitly modeling spatial relationships through graph neural architectures (Pourebrahim et al. 2018; Liu et al. 2020; Yao et al. 2020). Despite these advances, deployment remains challenging in data-scarce regions (Haraguchi et al. 2022; Cao et al. 2025b). More critically, no existing methodology maintains structural consistency under regional index permutations—a fundamental requirement for robust city-scale mobility synthesis that Sat2Flow addresses through its topology-agnostic design.

Conclusion

This work introduces Sat2Flow, a novel framework that generates high-fidelity OD flow matrices using only satellite imagery without requiring auxiliary urban data. By integrating multi-kernel encoding with contrastive learning and permutation-aware diffusion modeling, our approach preserves structural coherence under arbitrary regional index permutations while capturing both regional characteristics and global mobility patterns. Extensive experiments demonstrate that Sat2Flow outperforms state-of-the-art methods across multiple evaluation metrics, achieving 7.06% higher

CPC and 6.52% lower JSD under index permutations compared to the strongest baseline. The framework's ability to leverage universally accessible remote sensing data while maintaining structural consistency offers a scalable solution for urban mobility analysis in data-scarce regions.

Acknowledgments

This research was supported in part by Shenzhen Science and Technology Program (No. JCYJ20240813113300001, 20231127180406001, JYCJ20220530152817039, JCYJ20240813113218025).

References

- Axhausen, K. W.; Zimmermann, A.; Schönfelder, S.; Rindsfuser, G.; and Haupt, T. 2002. Observing the rhythms of daily life: A six-week travel diary. *Transportation*, 29(2): 95–124.
- Barbosa, H.; Barthelemy, M.; Ghoshal, G.; James, C. R.; Lenormand, M.; Louail, T.; Menezes, R.; Ramasco, J. J.; Simini, F.; and Tomasini, M. 2018. Human mobility: Models and applications. *Physics Reports*, 734: 1–74.
- Bojchevski, A.; Shchur, O.; Zügner, D.; and Günnemann, S. 2018. Netgan: Generating graphs via random walks. In *International conference on machine learning*, 610–619. PMLR.
- Calabrese, F.; Di Lorenzo, G.; Liu, L.; and Ratti, C. 2011. Estimating Origin-Destination flows using opportunistically collected mobile phone location data from one million users in Boston Metropolitan Area. *IEEE Pervasive Computing*.
- Cao, J.; Wang, X.; Chen, G.; Tu, W.; Shen, X.; Zhao, T.; Chen, J.; and Li, Q. 2025a. Disentangling the hourly dynamics of mixed urban function: A multimodal fusion perspective using dynamic graphs. *Information Fusion*, 117: 102832.
- Cao, J.; Wang, X.; Chen, J.; Tu, W.; Li, Z.; Yang, X.; Zhao, T.; and Li, Q. 2025b. Urban representation learning for fine-grained economic mapping: A semi-supervised graph-based approach. *ISPRS Journal of Photogrammetry and Remote Sensing*, 226: 317–331.
- Cao, J.; Wang, X.; Chen, J.; Zhang, B.; Ma, Y.; and Zhao, T. 2025c. SemiGPS: GraphGPS-based Semi-supervised Graph Learning for Sector-Specific GDP Mapping. In *ICASSP 2025-2025 IEEE International Conference on Acoustics, Speech and Signal Processing (ICASSP)*, 1–5. IEEE.
- Haraguchi, M.; Nishino, A.; Kodaka, A.; Allaire, M.; Lall, U.; Kuei-Hsien, L.; Onda, K.; Tsubouchi, K.; and Kohtake, N. 2022. Human mobility data and analysis for urban resilience: A systematic review. *Environment and Planning B: Urban Analytics and City Science*, 49(5): 1507–1535.
- Ho, J.; Jain, A.; and Abbeel, P. 2020. Denoising diffusion probabilistic models. *Advances in neural information processing systems*, 33: 6840–6851.
- Iqbal, M. S.; Choudhury, C. F.; Wang, P.; and González, M. C. 2014. Development of origin–destination matrices using mobile phone call data. *Transportation research part C: emerging technologies*, 40: 63–74.
- Joubert, J. W.; and De Waal, A. 2020. Activity-based travel demand generation using Bayesian networks. *Transportation Research Part C: Emerging Technologies*, 120: 102804.
- Liu, F.; Chen, D.; Guan, Z.; Zhou, X.; Zhu, J.; Ye, Q.; Fu, L.; and Zhou, J. 2024. Remoteclip: A vision language foundation model for remote sensing. *IEEE Transactions on Geoscience and Remote Sensing*, 62: 1–16.
- Liu, Z.; Miranda, F.; Xiong, W.; Yang, J.; Wang, Q.; and Silva, C. 2020. Learning geo-contextual embeddings for commuting flow prediction. In *Proceedings of the AAAI conference on artificial intelligence*, volume 34, 808–816.
- Luca, M.; Barlacchi, G.; Lepri, B.; and Pappalardo, L. 2021. A survey on deep learning for human mobility. *ACM Computing Surveys (CSUR)*, 55(1): 1–44.
- Mohanty, S. P.; Czakon, J.; Kaczmarek, K. A.; Pyskir, A.; Tarasiewicz, P.; Kunwar, S.; Rohrbach, J.; Luo, D.; Prasad, M.; Fleer, S.; et al. 2020. Deep learning for understanding satellite imagery: An experimental survey. *Frontiers in Artificial Intelligence*, 3: 534696.
- Pouerebrahim, N.; Sultana, S.; Niakanlahiji, A.; and Thill, J.-C. 2019. Trip distribution modeling with Twitter data. *Computers, Environment and Urban Systems*, 77: 101354.
- Pouerebrahim, N.; Sultana, S.; Thill, J.-C.; and Mohanty, S. 2018. Enhancing trip distribution prediction with twitter data: comparison of neural network and gravity models. In *Proceedings of the 2nd acm sigspatial international workshop on ai for geographic knowledge discovery*, 5–8.
- Pumain, D.; Paulus, F.; Vacchiani-Marcuzzo, C.; and Lobo, J. 2006. An evolutionary theory for interpreting urban scaling laws. *Cybergeography: European Journal of Geography*.
- Rombach, R.; Blattmann, A.; Lorenz, D.; Esser, P.; and Ommer, B. 2022. High-resolution image synthesis with latent diffusion models. In *Proceedings of the IEEE/CVF conference on computer vision and pattern recognition*, 10684–10695.
- Rong, C.; Ding, J.; Liu, Y.; and Li, Y. 2024. A large-scale benchmark dataset for commuting origin-destination matrix generation. arXiv:2407.15823.
- Rong, C.; Ding, J.; Liu, Z.; and Li, Y. 2023. Complexity-aware large scale origin-destination network generation via diffusion model. arXiv:2306.04873.
- Saberi, M.; Rashidi, T. H.; Ghasri, M.; and Ewe, K. 2018. A complex network methodology for travel demand model evaluation and validation. *Networks and Spatial Economics*, 18(4): 1051–1073.
- Shawe-Taylor, J.; and Cristianini, N. 2004. *Kernel methods for pattern analysis*. Cambridge university press.
- Simini, F.; Barlacchi, G.; Luca, M.; and Pappalardo, L. 2021. A deep gravity model for mobility flows generation. *Nature communications*, 12(1): 6576.
- Simini, F.; González, M. C.; Maritan, A.; and Barabási, A.-L. 2012. A universal model for mobility and migration patterns. *Nature*, 484(7392): 96–100.
- Song, J.; Meng, C.; and Ermon, S. 2020. Denoising diffusion implicit models. arXiv:2010.02502.

Wang, X.; Cao, J.; Zhao, T.; Zhang, B.; Chen, G.; Li, Z.; Chen, H.; Tu, W.; and Li, Q. 2025. ST-Camba: A decoupled-free spatiotemporal graph fusion state space model with linear complexity for efficient traffic forecasting. *Information Fusion*, 103495.

Yan, Y.; Wen, H.; Zhong, S.; Chen, W.; Chen, H.; Wen, Q.; Zimmermann, R.; and Liang, Y. 2024. Urbancip: Learning text-enhanced urban region profiling with contrastive language-image pretraining from the web. In *Proceedings of the ACM Web Conference 2024*, 4006–4017.

Yao, X.; Gao, Y.; Zhu, D.; Manley, E.; Wang, J.; and Liu, Y. 2020. Spatial origin-destination flow imputation using graph convolutional networks. *IEEE Transactions on Intelligent Transportation Systems*, 22(12): 7474–7484.

Zipf, G. K. 1946. The P 1 P 2/D hypothesis: on the intercity movement of persons. *American sociological review*, 11(6): 677–686.

Reproducibility Checklist

1. General Paper Structure

- 1.1. Includes a conceptual outline and/or pseudocode description of AI methods introduced (yes/partial/no/NA) **yes**.
- 1.2. Clearly delineates statements that are opinions, hypothesis, and speculation from objective facts and results (yes/no) **yes**.
- 1.3. Provides well-marked pedagogical references for less-familiar readers to gain background necessary to replicate the paper (yes/no) **yes**.

2. Theoretical Contributions

- 2.1. Does this paper make theoretical contributions? (yes/no) **no**.

If yes, please address the following points:

- 2.2. All assumptions and restrictions are stated clearly and formally (yes/partial/no) **NA**.
- 2.3. All novel claims are stated formally (e.g., in theorem statements) (yes/partial/no) **NA**.
- 2.4. Proofs of all novel claims are included (yes/partial/no) **NA**.
- 2.5. Proof sketches or intuitions are given for complex and/or novel results (yes/partial/no) **NA**.
- 2.6. Appropriate citations to theoretical tools used are given (yes/partial/no) **NA**.
- 2.7. All theoretical claims are demonstrated empirically to hold (yes/partial/no/NA) **NA**.
- 2.8. All experimental code used to eliminate or disprove claims is included (yes/no/NA) **NA**.

3. Dataset Usage

- 3.1. Does this paper rely on one or more datasets? (yes/no) **yes**.

If yes, please address the following points:

- 3.2. A motivation is given for why the experiments are conducted on the selected datasets (yes/partial/no/NA) **yes**.
- 3.3. All novel datasets introduced in this paper are included in a data appendix (yes/partial/no/NA) **no**.
- 3.4. All novel datasets introduced in this paper will be made publicly available upon publication of the paper with a license that allows free usage for research purposes (yes/partial/no/NA) **yes**.
- 3.5. All datasets drawn from the existing literature (potentially including authors' own previously published work) are accompanied by appropriate citations (yes/no/NA) **yes**.
- 3.6. All datasets drawn from the existing literature (potentially including authors' own previously published work) are publicly available (yes/partial/no/NA) **yes**.
- 3.7. All datasets that are not publicly available are described in detail, with explanation why publicly available alternatives are not scientifically satisfying (yes/partial/no/NA) **yes**.

4. Computational Experiments

- 4.1. Does this paper include computational experiments? (yes/no) **yes**.

If yes, please address the following points:

- 4.2. This paper states the number and range of values tried per (hyper-) parameter during development of the paper, along with the criterion used for selecting the final parameter setting (yes/partial/no/NA) **yes**.
- 4.3. Any code required for pre-processing data is included in the appendix (yes/partial/no) **no**.
- 4.4. All source code required for conducting and analyzing the experiments is included in a code appendix (yes/partial/no) **no**.
- 4.5. All source code required for conducting and analyzing the experiments will be made publicly available upon publication of the paper with a license that allows free usage for research purposes (yes/partial/no) **yes**.
- 4.6. All source code implementing new methods have comments detailing the implementation, with references to the paper where each step comes from (yes/partial/no) **partial**.

- 4.7. If an algorithm depends on randomness, then the method used for setting seeds is described in a way sufficient to allow replication of results (yes/partial/no/NA) [yes](#).
- 4.8. This paper specifies the computing infrastructure used for running experiments (hardware and software), including GPU/CPU models; amount of memory; operating system; names and versions of relevant software libraries and frameworks (yes/partial/no) [yes](#).
- 4.9. This paper formally describes evaluation metrics used and explains the motivation for choosing these metrics (yes/partial/no) [yes](#).
- 4.10. This paper states the number of algorithm runs used to compute each reported result (yes/no) [no](#).
- 4.11. Analysis of experiments goes beyond single-dimensional summaries of performance (e.g., average; median) to include measures of variation, confidence, or other distributional information (yes/no) [yes](#).
- 4.12. The significance of any improvement or decrease in performance is judged using appropriate statistical tests (e.g., Wilcoxon signed-rank) (yes/partial/no) [yes](#).
- 4.13. This paper lists all final (hyper-)parameters used for each model/algorithm in the paper's experiments (yes/partial/no/NA) [yes](#).